New measurements of the lifetimes of excited states of ^{55}Mn below 2.7 MeV

J. A. Caggiano,[1] R. D. Hasty,[2] S. E. Korbly,[2] W. H. Park,[2] and G. A. Warren[1]

[1]*Pacific Northwest National Laboratory, Richland, Washington 99352, USA*
[2]*Passport Systems Inc., Billerica, Massachusetts 01862, USA*

The lifetimes of the excited states of ^{55}Mn between 1.5 and 2.7 MeV were measured using nuclear resonance fluorescence. The absolute lifetimes of the excited levels were determined from simultaneous measurements of manganese and aluminum. In this approach, the precisely known aluminum state serves as a means to normalize the results. Our findings differ from the evaluated level lifetimes in the Evaluated Nuclear Structure Data File (ENSDF), but agree with earlier nuclear resonance fluorescence measurements.

Nuclear resonance fluorescence (NRF) provides an isotopic-specific signature that can be used to detect and characterize isotopes within a sample. In this process, a nucleus is excited by an incident photon, and the γ rays from the subsequent decay of that nucleus are detected. NRF has the potential to address a wide range of needs, such as characterization of radioactive waste, detection of illicit materials, and characterization of nuclear fuel. Given this potential, a significant effort has been made to understand the NRF response of special nuclear materials, such as ^{235}U and ^{239}Pu.

Earlier measurements of the nuclear resonance fluorescence (NRF) response of ^{235}U were made using manganese as a means to normalize the absolute flux [1]. The 1884-keV level of ^{55}Mn served as a means to determine the absolute strength of the ^{235}U NRF response. The lifetime of this level has been measured by Alston *et al.* [2] using NRF techniques.

There are some difficulties with the Alston data. First, they observed a significantly different branching ratio for the decay from the 1884-keV level than reported recently in the Nuclear Data Sheets [3]. Second, while the lifetime of the 1884-keV state reported in Alston *et al.*, 9.1 ± 1.3 fs, does not differ significantly from that reported in Ref. [3], 12 ± 3 fs, it does differ significantly from the lifetimes determined from different reactions that form the evaluated lifetime in Ref. [3]. The evaluated lifetime of the 1884-keV level of ^{55}Mn in Ref. [3] is based on evaluated lifetimes using three different reactions: 9 ± 2 fs from $(n,n'\gamma)$, 19 ± 3 fs from $(p,p'\gamma)$ and 11 ± 8 fs from $(p,p'\gamma)$. The significant variation of the lifetimes from these different reactions is unsatisfactory. Based on the differences of the Alston data and the reaction-based lifetimes used in Ref. [3], we felt it prudent to conduct a new measurement to accurately determine the lifetime of the 1884-keV state of ^{55}Mn, as well as the neighboring states of ^{55}Mn, using the (γ,γ') reaction.

Our measurement of this lifetime is based on NRF techniques using bremsstrahlung radiation. The NRF response of a manganese target and an aluminum target were measured simultaneously. The absolute NRF cross sections of the Mn transitions are extracted from the relative response of the manganese and aluminum. The aluminum NRF response has been extensively and carefully measured [4]. By measuring ratios of observables, our approach reduces sensitivities to

certain systematic uncertainties. While this ratio approach may not provide uncertainties as low as those achieved through the self-absorption approach, such as used in Ref. [4], it does provide a means to accurately measure the lifetimes of states for isotopes in which one is limited in the configurability of the material. This report discusses the measurements, the data analysis, and a comparison of the lifetimes from this measurement to those previously published.

The measurements were conducted in December 2006 at the High Voltage Research Laboratory (HVRL) at the Massachusetts Institute of Technology. The experimental facilities for conducting NRF measurements at the HVRL were set up by Passport Systems. The experimental setup is shown in Fig. 1.

The HVRL uses a 4-MeV Van de Graff electron accelerator. For these measurements, the accelerator ran at 2.8 MeV with an average current of 10.8 μA. After a 90° bend, the beam is directed into a converter to produce a bremsstrahlung photon beam. The converter consists of 0.1 mm of Au followed by 10 mm of copper. The converter is surrounded by 8 in. of lead, with an approximately 2.5° conical collimator.

The collimated bremsstrahlung photon beam was incident on the targets 69.8 cm downstream from the converter. The photon beam was aligned by steering the electron beam on the radiator and observing the x-ray image with a Perkin-Elmer imager (not shown in Fig. 1) downstream of the target. The targets consisted of 3.5-in.-diameter disks of aluminum and manganese, weighing 212.6 and 220.0 g, respectively. Measurements were conducted both with the manganese as the upstream material and then with the aluminum as the upstream material.

The detectors consisted of two high-purity germanium detectors of approximately 100% relative efficiency. The detectors were placed at 120° with respect to the beam and 42 cm away from the center of the targets. An 8-in. lead cave surrounded the detectors on all sides, except for the side facing the target. A 3/4 in.-thick lead filter was placed in front of the detectors to reduce the low-energy photon count rate from the targets. The data were acquired using ORTEC DSpec-Pro data acquisition hardware in histogram mode.

Absolute calibrations were conducted using the ^{27}Al 2212-keV line within the observed spectra. This approach enables the testing of the entire measurement system under
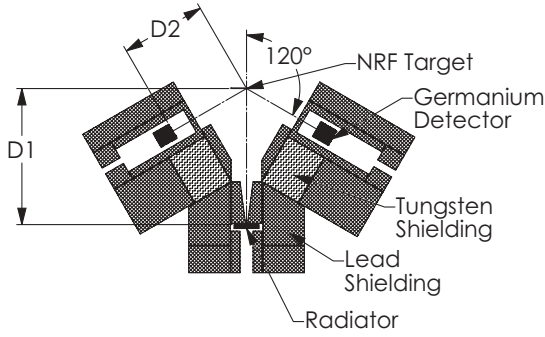
FIG. 1. Diagram of experimental setup. The electron beam is coming from the bottom of the figure toward the radiator. For this measurement, $D1 = 69.8$ cm, $D2 = 42.0$ cm.

the same conditions as the physics measurement. For instance, pileup issues were similar for both the calibration and physics data. The rates of the 2212-keV line for both the aluminum plate upstream and downstream of the manganese plate were consistent well within uncertainties of the measurement, which are discussed later.

The spectrum from the measurement with the manganese upstream of the aluminum is shown in Fig. 2. Many of the excited states of ^{55}Mn decay to both the ground state and 125.9-keV excited state. This splitting produces two lines for the same excitation energy.

The observed counts can be decomposed into the following terms related to the measurement:

$$N = \phi(E_x)T_{in}(E_x)C_{thick}\frac{W(\theta)}{4\pi}T_{out}(E_\gamma)\varepsilon(E_\gamma)\Delta\Omega, \quad (1)$$

where $\phi(E_x)$ is the photon current incident on the target, $T_{in}(E_x)$ is the transmission probably for photons of energy E_x to pass through any materials between the photon source and the target, C_{thick} is the number of fluorescent photons per incident flux escaping the target, $T_{out}(E_\gamma)$ is the transmission probability of the outgoing photon passing undisturbed through any materials between the target and the detector, $(W\theta)/4\pi$ is the angular distribution of the resonant photons, $\varepsilon(E_\gamma)$ is the detector photopeak efficiency for a photon of energy E_γ, and $\Delta\Omega$ is the solid angle of the detector.
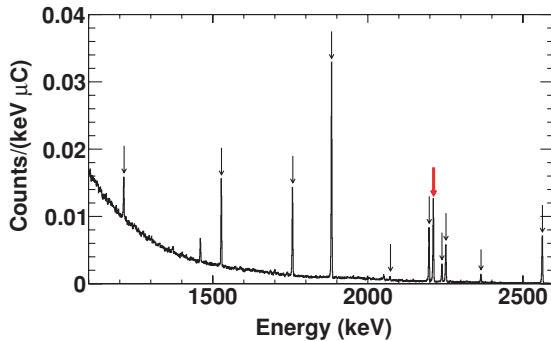

FIG. 2. (Color online) Spectrum from Mn upstream of Al measurement. The ^{55}Mn and ^{27}Al resonances are indicated with arrows. The ^{27}Al line at 2212 keV is denoted with a thicker red arrow.

C_{thick} is related to the probability of generating a resonant photon in the direction of the detector from the target material. In the limit of a thin target in which attenuation is unimportant, C_{thick} reduces to the energy integral of the cross section times to nuclei/area of the target material. It accounts for both electronic and resonant attenuation for the incident photon, the probability of generating a resonant photon and electronic attenuation for the exiting resonant photon in the target material. The calculation assumes that the target is a thick plate, but does not correct for possible edge effects, which are small for the geometry of these measurements. C_{thick} does not include the angular dependence of the transition, but it does depend on the angle of the detector in order to determine attenuation of the outgoing photon through the target material. The analytical calculation for C_{thick} is taken from Metzger [5], except that we have explicitly factored out the photon flux because it is constant over the Doppler width of the resonances. In this manner, our C_{thick} is in units of number of resonant photons escaping the target per incident photon per eV. C_{thick} properly accounts for the potentially nonlinear attenuation effects as a function of energy over the resonance. For thin targets, these nonlinear effects are less important. C_{thick} also accounts for the thermal broadening of the resonance by assuming that the resonance is shaped by convolution of the Maxwellian distribution for the thermal broadening with the Breit-Wigner shape of the resonance.

C_{thick} is sensitive to the NRF cross section in an almost linear manner. The larger the cross section, the more significant the attenuation of the incident beam and the less linear the relationship. Once C_{thick} is determined from the data, the lifetime of the level can be extracted using the branching ratios, the Doppler width, the spin of the states involved, and the energy of the resonance.

The product of terms $T_{out}(E_\gamma)\varepsilon(E_\gamma)\Delta\Omega$ was determined through simulations using the GEANT4 (G4) framework [6]. As the attenuation of the resonant photons in the target material are addressed in the C_{thick} calculation, the target material was assumed to be a vacuum. Reduction in the production of the resonant photons as function of the beam penetration depth into the sample was approximated by an exponential dependence.

The first step in deducing the level lifetimes is to determine the branching ratios for those excited states with multiple decay paths using the following relationship based on Eq. (1):

$$\frac{C_{thick}^1}{C_{thick}^2} = \frac{N_1/W_1 T_1^{out}(E_1)\varepsilon(E_1)}{N_2/W_2 T_2^{out}(E_2)\varepsilon(E_2)}, \quad (2)$$

where subscripts 1 and 2 indicate the two different photon energies. All other terms in Eq. (1) are the same for the observed photons originating from the same excited state. The level lifetimes were adjusted in the calculations of C_{thick} until the extracted C_{thick}^1/C_{thick}^2 ratio agreed with the measured value. For the branching ratio determination, only the configuration with the manganese upstream of the aluminum was used, because that geometry involved the least attenuation of the Mn resonance lines. A listing of the extracted branching ratios, as well as those currently reported in Ref. [3], is shown

TABLE I. Branching ratios for ^{55}Mn determined from this paper and as reported in Ref. [3].

Energy (keV)	Current work	Ref. [3]
1402	0.030 ± 0.012	0.034 ± 0.004
1528	0.970 ± 0.012	0.97 ± 0.01
1758	0.290 ± 0.005	0.36 ± 0.09
1884	0.710 ± 0.005	0.64 ± 0.03
1214	0.380 ± 0.014	0.33 ± 0.02
2072	0.036 ± 0.007	0.06 ± 0.02
2198	0.584 ± 0.014	0.61 ± 0.04
2239	0.662 ± 0.015	0.74 ± 0.02
2365	0.338 ± 0.015	0.26 ± 0.06

in Table I. The results are similar to, but slightly different from, the evaluated branching ratios reported in Ref. [3]. For consistency, the branching ratios extrapolated from our data were used to determine the level lifetimes.

The ratio of C_{thick}'s for a ^{55}Mn peak and the ^{27}Al peak is related to the relative strength of the observed peaks by the ratio of two corresponding versions of Eq. (2). All factors relating the observed signal strength to the ratio of C_{thick}'s are ratios. These ratios were determined through a variety of means. The ratio of counts is determined from the observed spectrum. The relative photon flux was determined from the G4 simulations. The T_{in} terms were determined from the number of attenuation lengths, as determined from the XCOM cross section [7], of the material upstream. The angular distributions were determined following Ref. [8]. The ratio of the final three terms, the transmission out, the detector efficiency, and the solid angle, was determined through G4 simulations, as discussed earlier.

An absolute determination of $C_{\text{thick}}^{\text{Al}}$ was necessary to extract the value of $C_{\text{thick}}^{\text{Mn}}$. $C_{\text{thick}}^{\text{Al}}$ was determined from the cross sections reported in Ref. [4] and found to be 1.035 ± 0.027 eV. The uncertainty was determined from two components added in quadrature: the uncertainty of the lifetime measurement [4] and the uncertainty from a possible uncertainty of $\pm 10\%$ in the electronic cross section. The latter part would lead to different attenuation in the target. The two components were roughly equal.

The lifetimes of the ^{55}Mn states were then determined from the absolute values for $C_{\text{thick}}^{\text{Mn}}$. Given the parameters of the measurement, the lifetime of the state and the evaluated $C_{\text{thick}}^{\text{Mn}}$ have a one-to-one relationship, so that by inverting this relationship one can determine the lifetime from C_{thick}. Likewise, the uncertainties in the lifetime due to the uncertainties in C_{thick} can be determined in a similar manner.

This inversion process addresses the possible amplification of the uncertainty of the lifetime because of saturation in the target. If saturation was significant, then C_{thick} would vary little for large changes in the lifetime. This weak dependence would produce large uncertainties in the lifetime. This saturation effect was not significant for this measurement. For instance, for the 1884-keV line, the relative uncertainty in C_{thick} is 6.5% while the relative uncertainty in the lifetime is 8.2%,

suggesting that despite the rather thick targets the signal rate is not saturated for this measurement.

Systematic uncertainties in the lifetime are minimized by using ratios of quantities. With the exception of the $C_{\text{thick}}^{\text{Al}}$, only relative quantities were used to determine the lifetime of the ^{55}Mn states. For instance, the approach is not sensitive to the absolute detector efficiency of the 1884-keV line but rather the relative efficiency of the 1884-keV line of ^{55}Mn and the 2211-keV line of ^{27}Al. Likewise, the extraction of the lifetimes depends not on the absolute photon flux, but on the relative photon flux at two different energies. These relative dependences greatly reduce the systematic uncertainties.

A breakdown of the contributions to the uncertainty in C_{thick} is shown in Table II. The uncertainty of the ratio of counts was statistical. The uncertainty in the ratio of photon flux was determined by varying the bremsstrahlung end-point energy from 2.7 to 2.9 to determine the change in the ratio of fluxes. No uncertainty was accounted for in the ratio of T_{in}. Uncertainties in the electronic cross sections most significantly impact $C_{\text{thick}}^{\text{Al}}$, which does not involve a ratio; this uncertainty was discussed earlier. For the angular dependence, no uncertainty was accounted for when mixing parameters for both the initial and final transitions were known. For the 2252-keV state, for which the mixing parameter is unknown, the ratio was determined assuming the mixing parameter was 0 and the uncertainty was taken as the largest difference for variation of the mixing parameter of ± 0.30. This uncertainty was 2.1%. Uncertainties related to the branching ratio were determined by varying the branching ratio in the calculation of C_{thick}. Finally, the uncertainty of the transmission out times the detection efficiencies was determined by varying the HPGe crystal dimensions by $\pm 10\%$ in the simulations as a means to estimate the upper limit of the uncertainty in detector efficiency.

Despite these conservative estimates for the uncertainties, the uncertainties in the ratios remain fairly small. For instance, the $\pm 10\%$ variation in detector size used to estimate the sensitivity to the detection efficiency yields an ~40% uncertainty in the absolute rate for an individual resonance but only $\leqslant 2.3\%$ uncertainty in the relative yields of two different resonances. This reduction in the uncertainty demonstrates the systematic advantage of conducting relative measurements.

C_{thick} for each ^{55}Mn line were determined from the two target geometries, Mn upstream of Al and Al upstream of Mn. Results from these two geometries, which were consistent, were averaged to form the central values for $C_{\text{thick}}^{\text{Mn}}$. The uncertainties were determined by adding, in quadrature,

TABLE II. Relative uncertainty contributions to C_{thick}.

Energy (keV)	Statistics (%)	Photon flux (%)	Det. eff. (%)	Br. ratio (%)
1528	3.8	5.0	2.3	2.9
1884	2.6	3.8	1.9	1.6
2198	3.6	0.3	0.3	5.0
2252	4.0	0.9	0.3	–
2365	6.4	4.2	0.3	2.1
2563	3.7	16.0	1.4	–

TABLE III. Lifetimes of states determined from this paper, from Alston *et al.* using our branching ratios, and reported in Ref. [3].

Energy (keV)	This paper (fs)	Alston (fs)	Ref. [3] (fs)	Consistency with Ref. [3]
1528	52.6 ± 5.1	61 ± 25	62 ± 12	1 of 3
1884	7.78 ± 0.64	9.6 ± 1.0	12 ± 3	2 of 3
2198	10.91 ± 0.92	26.1 ± 5.8	18 ± 6	2 of 4
2252	19.2 ± 1.1	26.0 ± 5.8	23 ± 2	2 of 4
2365	12.46 ± 1.0	14.8 ± 5.3	23 ± 2	0 of 3
2563	5.66 ± 0.86	5.0 ± 1.0	7.7 ± 1.4	2 of 3

one-half of the difference between the central values of the two target geometries and the uncertainties of the weighted mean of values. C_{thick} value. The extracted values for the lifetimes are presented in Table III. The lifetimes for decays of the same excited state to different final levels were consistent. This agreement is a self-consistency check between the branching ratio results, determined from the Mn upstream data, and the lifetime results, determined from both geometry data.

It is possible that higher energy states feed into the response of lower energy states. With an end-point energy of 2.8 MeV, there are only two possible states that could feed into a level discussed in this paper: the 2426.5- and 2266.8-keV levels can both have decays paths to the 1528.4-keV level according to Ref. [3]. The contribution from these states to the 1528.4-keV level are estimated at 0.2% and 0.5%, respectively. Both of these contributions are small compared to the uncertainties and have been ignored.

The level lifetimes we deduced differ from the evaluated lifetimes reported in Ref. [3]. However, those values are derived from the evaluated lifetimes determined from various reactions. As discussed earlier for the 1884-keV line, some of those reaction-based evaluated lifetimes vary considerably. We checked the consistency of our results with the reaction-based evaluated lifetimes used to form the evaluated lifetime in Ref. [3]. Our findings, which show consistency with some of the reaction-based lifetimes, are reported in the last column of Table III.

Our results are largely consistent with corrected lifetimes of Alston *et al.* The Alston *et al.* results were corrected for our observed branching ratios and for the proper angular momentum factors now that the spins of the levels are known. Five out of the six lifetimes agree within 1.5σ; whereas the sixth lifetime, for the 2198-keV level, differs by 2.5σ. While within agreement to the existing data on a point-by-point basis, our results are systematically lower than prior results.

We have presented results on new measurements of the lifetimes of the excited states of ^{55}Mn below 2.7 MeV accessible via the (γ, γ') reaction. The measurements utilized an approach allowing for the extraction of these excited states by comparing to the well-known 2212-keV line of ^{27}Al. This ratio method reduces sensitivities to many of the systematic uncertainties. Our results are largely consistent with prior results and provide reduced uncertainties. While this technique may not provide enhanced precision of level lifetime measurements compared to NRF self-absorption techniques, our results indicate that it does provide suitable precision for materials in which one is limited in configurability for conducting measurements.

[1] W. Bertozzi *et al.*, Phys. Rev. C **78**, 041601(R) (2008).

[2] W. J. Alston III, H. H. Wilson, and E. C. Booth, Nucl. Phys. **A116**, 281 (1968); **A139**, 713 (1968).

[3] Huo Junde, Nucl. Data Sheets **109**, 787 (2008).

[4] N. Pietralla *et al.*, Phys. Rev. C **51**, 1021 (1995).

[5] F. R. Metzger, in *Progress in Nuclear Physics*, edited by O. R. Frisch (Pergamon Press, New York, 1959), pp. 54–88.

[6] S. Agostinelli *et al.*, Nucl. Instrum. Methods A **506**, 250 (2003); J. Allison *et al.*, IEEE Trans. Nucl. Sci. **53**, 270 (2006).

[7] M. J. Berger *et al.*, http://physics.nist.gov/xcom.

[8] H. Frauenfelder and R. M. Steffen, *Alpha-, Beta-, and Gamma-Ray Spectroscopy*, edited by K. Siegbahn (North-Holland, Amsterdam, 1965), Vol. 2, p. 997.